



## SYSTEM-LEVEL FRAGILITY ASSESSMENT UNDER INTERDEPENDENT SPATIAL DEMAND AND STRUCTURAL CAPACITY

C. Zelaschi<sup>(1)</sup>, M. Pozzi<sup>(2)</sup>, R. Monteiro<sup>(3)</sup>, C. Malings<sup>(4)</sup>

<sup>(1)</sup> PhD student, ROSE Programme, UME School Pavia, Carnegie Mellon University (visiting scholar), [claudia.zelaschi@umeschool.it](mailto:claudia.zelaschi@umeschool.it)

<sup>(2)</sup> Assistant Professor, Carnegie Mellon University, Pittsburgh, [mpozzi@cmu.edu](mailto:mpozzi@cmu.edu)

<sup>(3)</sup> Assistant Professor, IUSS Pavia, Pavia, [ricardo.monteiro@iusspavia.it](mailto:ricardo.monteiro@iusspavia.it)

<sup>(4)</sup> PhD student, Carnegie Mellon University, Pittsburgh, [cmalings@andrew.cmu.edu](mailto:cmalings@andrew.cmu.edu)

### **Abstract**

Seismic risk assessment is more challenging for infrastructure systems than for single, non-interacting components, especially when network-level interaction is included in the analysis. Accounting for the interdependencies of the spatially distributed demands and of the capacity does significantly affect reliability and risk assessment. The spatial distribution of the ground motion intensity is one of the main sources of dependences among the components' response, and models for predicting the correlation of the most commonly used intensity measures (peak ground acceleration, spectral acceleration at the fundamental period of vibration, spectral acceleration at multiple periods, etc.) at different locations are available in literature. However, when these models are applied to system-level analysis, it is still to be determined if the capacity of different components (modelled by the fragility function) should be considered as dependent or independent. Dependence can derive from two sources: on one hand, epistemic uncertainty can be common across many components, on the other, the seismic intensity may be just an incomplete summary of the seismic event, not able to capture relevant features of the demand. Because of this, an assessment of the response that only accounts for the interdependence in the seismic intensity may underestimate the actual dependence. To investigate such a loss of information about the correlation between structural responses, we perform non-linear analyses of a RC bridge, using sets of ground motions recorded during the same event at two different locations, and compare actual and predicted interdependence. From the simulations' results, we investigate the accuracy of system-level analysis.

*Keywords: system-level analysis, spatially distributed structures, RC bridges*



## 1. Introduction

Seismic risk analysis at network-level is crucial for post-event loss assessment of infrastructures' critical components, whose damage state level in the immediate aftermath of an earthquake can significantly affect the management of the emergency phases. Moreover, severe past seismic events, such as L'Aquila (2009), Christchurch (2011) and Ecuador (2016), have demonstrated the catastrophic human and economic impact that road network systems' damage or collapses can cause. Bridges are among the most vulnerable road point-site components [1, 2] and they play an important role in ensuring the efficient functionality of the network itself. Therefore, the accuracy of their damage level estimation is crucial to assessing the state of the system.

It is common practice to characterize the physical vulnerability of such structures by using fragility curves. Fragility curves are conditional probability tools that estimate the probabilities of exceeding certain damage limit states (DLSs) for different given intensity measure (IM) levels, where the conditioning parameter is typically a scalar intensity measure. They can be obtained (among other methodologies) through nonlinear response analyses. A number of past studies [3, 4] provided fragility curves for different types of individual structures, and further research aimed to scrutinize aspects that were not covered by the previous generation of fragility curves, such as the effects of including retrofit measures, irregularities, different abutment types, bridge skew angle, and cumulative damage after the main shock [5, 6, 7, 8]. However, the earthquake engineering community has increased their interest in studying the response of either individual bridge structures or bridge populations under seismic actions. In order to address the vulnerability assessment of heterogeneous bridge populations, fragility curves were derived by including a greater pool of structural configurations grouped into bridge classes [9]. When dealing with spatially distributed structures, a fragility function, which is representative of a broad class, is usually assigned to each individual structure, and possible capacity dependencies are not taken into account. Therefore, even though reliable fragility curves can be derived for the individual structure, they represent marginal probabilities, which do not necessarily reflect damage estimates of a system of structures, which remains a subject for investigation.

Once the optimal IM for the considered structures has been selected among the wide variety available in literature [10], some issues need to be considered. First of all, a methodology which defines the spatial correlation dependencies of the considered IM to be assigned at the structures' locations needs to be available. Secondly, in order to investigate the vulnerability of the different structures through nonlinear response analyses, sets of earthquake records are to be consistently selected. Such an aspect is not straightforward if the only information available at each location are scalar IMs (or vectors made up of scalar IMs). Indeed, the corresponding time histories cannot be drawn from such summary ground motion characteristics. However, for convenience, they are still frequently adopted given the availability of ground motion prediction equations (GMPEs) for such variables (peak ground acceleration, peak ground velocity, spectral acceleration at the fundamental period of vibration, etc.) and the fact that a significant amount of national seismic hazard information is still expressed in terms of these commonly employed IMs.

The current methodologies available to characterize the spatial distribution of IMs over a region are related to the quantification of correlations among residual spectral accelerations at the same spectral period at two different locations [11-15]; where the residual refers to the difference between the recorded ground motion parameter and the one predicted by the GMPE. More recently, some research [16] focused on the cross-correlations between spectral accelerations at different fundamental periods, which can be particularly useful for the seismic risk assessment of infrastructure portfolios, is being carried out. The general framework behind such studies is associated with GMPEs, in which the logarithm of the ground motion parameter of interest is obtained as a function of the logarithm of the predicted (by the adopted GMPE) median ground motion intensity and of different parameters such as magnitude, distance, period and soil type conditions. Intra-event and inter-event residuals are also included along with standard deviations which depend on the spectral period of interest [16]. However, since past research has demonstrated that other IMs may be more appropriate to define the link between seismic hazard and structural response, further studies have explored additional IMs. Foulser-Piggot and Stafford [17] focused on the spatial correlation of Arias intensity, and Esposito and Iervolino [18] used European earthquake data in order to investigate the spatial correlation of PGA and PGV. Yet, even if the selection of the aforementioned IMs is convenient for practical purposes (availability of GMPEs, National Seismic Hazard information given in terms of such IMs, etc.), they do not reflect the full set of ground motion time history characteristics and dependencies at different locations. One way to overcome such drawbacks is considering Power Spectral Density (PSD) functions as a



complete description of seismic excitation at different locations in a region. PSD functions provide a consistent and effective representation for processing heterogeneous time-history data, as they are intrinsically related to Gaussian process, which have the capability to describe the spatially distributed phenomenon (i.e. ground motion) as well as its uncertainty. The seismic excitation (e.g. the ground acceleration) during an earthquake can be intended as the realization of a spatio-temporal random field. For such reasons, in the present paper, the ground motion variability in the frequency domain is characterized by the model presented by Der Kiureghian [19] and Konakli and Der Kiureghian [20]. Such a model guarantees the spatial correlations of the seismic input and the possibility of simulating earthquake input sets at different locations. Even though the use of such methodology allows us to include input correlations, the prevalent practice in bridge network seismic reliability studies assumes independence among bridge failures.

The main focus of this work is to explore the damage dependences of structures at different locations given a specific seismic scenario by considering a case study. It should be mentioned that when time history information is summarized by a unique IM for each structure, the implicit assumption is that only the selected IM at the different locations is representative of the structural damage, i.e., all other properties of the ground motion are independent given the IM. However, the authors believe that, through this simplification, important information about the correlation between structural responses among spatially distributed structures of a similar type is being lost, and therefore that system-level damage estimates based on this methodology may be inaccurate [21]. This paper supports this claim by illustrating the contradiction between the assumption of independence and the results of simulations on a pair of bridges subjected to a common seismic event.

## 2. Spatial cross-correlation models and record simulations

To simulate spatially varying ground motions, the present work adopts the methodology presented in Konakli and Der Kiureghian [20]. The frequency-dependent coherency function characterizes the ground motion variability in the frequency domain, accounting for the incoherence effect, defined as the loss of a seismic wave's coherency due to wave propagation in the heterogeneous medium and the superposition of waves originated from different locations of the same seismic source. The general form of the coherency includes the phase angles that refer to the wave-passage and site-response effects, which are representative of a temporal wave shift. For the purpose of this study, they can be neglected since it is not relevant to capture the system's components' response when they are subjected to seismic actions at the same time. The adapted expression for the coherency, which refers to locations  $\alpha$  and  $\beta$ ,  $\gamma_{\alpha\beta}(\omega)$ , is given by Eq. (1):

$$\gamma_{\alpha\beta}(\omega) = \exp \left[ - \left( \frac{ad_{\alpha\beta}\omega}{v_s} \right)^2 \right] \quad (1)$$

$d_{\alpha\beta}$  is the distance between the sites  $\alpha$  and  $\beta$ ,  $v_s$  is the average shear wave velocity of the ground medium along the travel path, and  $a$  is the incoherence coefficient that can be empirically estimated from data or evaluated according to soil properties and depth of layers.

The formulated coherency function relates the cross-PSD,  $G_{\alpha\beta}(\omega)$  and the corresponding auto-PSDs  $G_{\alpha\alpha}(\omega)$  and  $G_{\beta\beta}(\omega)$ , according to Eq. (2).

$$G_{\alpha\beta}(\omega) = \gamma_{\alpha\beta}(\omega) [G_{\alpha\alpha}(\omega)G_{\beta\beta}(\omega)]^{\frac{1}{2}} \quad (2)$$

Auto-PSDs and cross-PSDs defines zero-mean jointly stationary Gaussian acceleration arrays of processes. In particular, such processes are represented in terms of Fourier series, at different locations, Auto-PSDs and cross-PSDs are used to determine all the Fourier coefficients.

## 3. System reliability analysis

The typically adopted approach for evaluating the structural seismic vulnerability of broad areas is to assign to each structural location an IM level, which is turned into the associated expected structural damage through the appropriate fragility curve. Within such a procedure the spatial correlation between IMs at different sites can be included according to the most recent studies available in literature. However, the available approaches consider only one IM, such as peak ground acceleration (PGA), spectral acceleration at the fundamental period of vibration ( $S_a(T)$ ) or spectral accelerations at different fundamental periods



( $Sa(T_i)$ ). These correlation models implicitly assume independence among the other ground motion characteristics at the different locations. The authors demonstrate that this simplification leads to the loss of important information of the input itself and of the correlation between structural responses among spatially distributed structures of a similar type.

### 3.1 Theoretical formulation

To illustrate this on a simple example, a series and a parallel system of two structures are considered. The model described in Section 2 can be used to generate a set of independent earthquake record simulations derived from a certain seismic scenario at different sites, to which a PSD function corresponds. From each simulation, IM values can be extracted and associated to the structural damage state, which can be obtained through finite element dynamic nonlinear analyses or more simplified procedures, such as static nonlinear analyses. The  $i$ -th bridge's state under a certain seismic scenario, and associated with a certain DLS, can be described by the variable  $s_i$ , which can take values 1 or 0 as indicated in Eq. (3).

$$s_i = \begin{cases} 1, & \text{if the bridge exceeds the considered DLS} \\ 0, & \text{otherwise} \end{cases} \quad (3)$$

Three possible system's states can occur: both structures are damaged or undamaged or only one of the two is damaged. If the system's damage condition is described by the variable  $s_{sys}$  of Eq. (4), it can take values from 0 to 2.

$$s_{sys} = s_1 + s_2 = \begin{cases} 0, & \text{if the bridges do not exceed the considered DLS} \\ 1, & \text{if one bridge exceeds the considered DLS} \\ 2, & \text{if both bridges exceed the considered DLS} \end{cases} \quad (4)$$

The one bridge's marginal probability of exceeding the DLS,  $p_f$ , can be expressed by Eq. (5), knowing the joint probabilities associated with the three system's states,  $p_{s_{sys}}$ :

$$\begin{cases} p_f = p_2 + p_1 \\ \rho = \frac{p_0 p_f^2 - p_1(1-p_f)p_f + p_2(1-p_f)^2}{p_f(1-p_f)} \end{cases} \quad (5)$$

$p_1$ , which is the probability that one of the two bridges exceeds the DLS, is defined by Eq. (6) as the average probability of one of the two bridges being damaged, and  $\rho$  is the correlation coefficient.

$$p_1 = \frac{1}{2} [p(0; 1) + p(1; 0)] \quad (6)$$

Where  $p(i; j) = P[s_1 = i; s_2 = j]$  is the probability that the first bridge is in state  $i$  and the second in state  $j$ .  $p_i = P[s_{sys} = n]$  is the probability that  $n$  bridges exceed the considered DLS.

The probability of the system in series being damaged can be defined according to Eq. (7). Eq. (8) refers to the system in parallel. In particular, in the last case, the system can be considered damaged (at the considered DLS) if both bridges exceed the DLS.

$$p_{series} = 1 - p_0 \quad (7)$$

$$p_{parallel} = p_2 \quad (8)$$

### 3.2 Comparison between time-history-based and IM-based methods

The system reliability assessment is addressed by comparing two methodologies aimed to estimate the system's damage, namely time-history-based and IM-based methods. The first approach assumes the availability of an adequate methodology to generate spatially correlated time history records consistent with a seismic scenario. It guarantees correlations between time history records and, consequently, between different associated IMs at different locations in a probabilistic fashion, by using the PSD and coherency function. One IM can be selected as the optimal variable that connects seismic hazard and the damage estimate, which can be obtained through fragility curves. The second approach is based on the belief that correlated IMs at different locations are capable of accurately providing information about the system's damage level. Indeed, once the optimal IM is chosen, available IM-based spatial correlation models are used

to assign to each considered site the appropriate IM value. In order to simulate this approach, the authors do not use any formulation to define the IM field; they instead resample IMs from the data obtained through the first approach, a technique which is valid since such IMs derive from simulated correlated ground motion records. IMs at different locations are therefore known and consistent time histories, which do not necessarily correspond to the same seismic scenario, can be drawn from a database. Damage state estimation is then done as above.

Summarizing, the time-history-based approach represents a more accurate way to estimate the system damage as the seismic input correlations are included in the procedure, keeping track of the entire earthquake record. The IM-based approach can be seen as a simplified approach that simulates the approximations resulting from reducing earthquake time-histories to one IM when evaluating the damage estimate. The comparison of the two approaches indicates how the damage correlation information is lost when the IM-based methodology is used.

To accomplish this comparison, from the time-history-based approach, a dataset consistent with a seismic scenario, containing time-history records, the corresponding IMs and the damage states,  $s$ , can be generated. In particular, the initial dataset can be transformed into a new dataset of resampled data: for each simulation of the initial dataset, the IMs at each location are considered and the closest IM at each location is independently identified within the main dataset. These IMs will be part of the resampled dataset together with the corresponding bridge damage states. The system's marginal probabilities of exceeding the considered DLS and the correlation factors can be recomputed from the resampled dataset. Their comparison with respect to the main dataset probabilities and correlation factor outcomes provides a quantification of the loss in terms of correlation, i.e. the correlation which is lost by summarizing the time history properties in one IM. If different IMs are considered, the best IM in predicting the damage can be identified as the one with a lower correlation loss.

The immediate application of this procedure is to evaluate the system's sampled damages in a deterministic fashion for simple systems in series and parallel, by including seismic input correlation. From a seismic scenario, coherent time histories can be simulated at different locations and they can be used to extract the associated damage, without the use of fragility curves, as illustrated in Fig. 1.

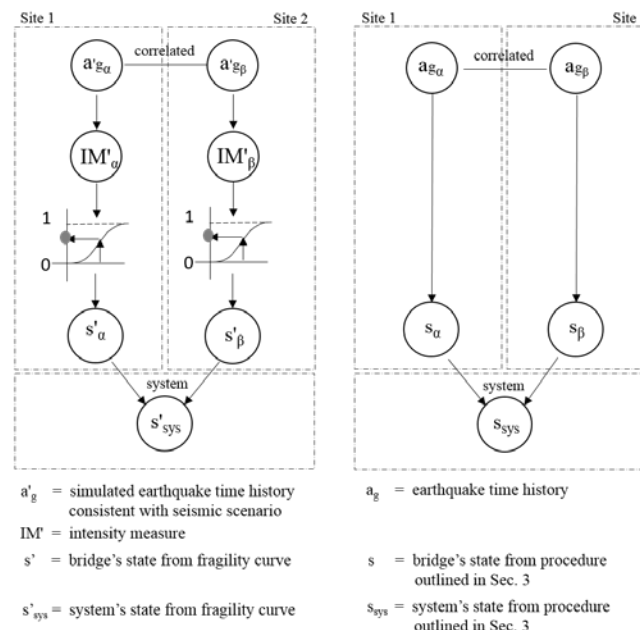


Fig. 1 – System's damage evaluation through fragility curves (left) and proposed approach (right) at two sites, namely  $\alpha$  and  $\beta$

#### 4. Case study

In order to explore the vulnerability correlation of structures at different locations, given a specific level of IM, this work focuses on two site locations 100m apart, namely  $\alpha$  and  $\beta$ . As a first approach, the extreme

case of two identical viaducts located in the two sites and the same soil conditions, characterized by a shear wave velocity of 800m/s, was considered.

The bridge typology selected for the case study, represented in Fig 2, is located in Italy, in the Marche region, an area characterized by the design response spectrum of Fig. 3 left, from which the corresponding PSD has been computed. The PSD function became the input of the procedure described in Section 2 through which, by including the coherency function, two sets of 100 earthquake seismic records have been simulated for the two sites, considering zero-mean, jointly stationary Gaussian acceleration arrays of processes at the two sites, defined by auto-PSD  $G_{kk}(\omega)$  and cross-PSD  $G_{kl}(\omega)$ , and represented in terms of Fourier series. The response spectra associated with the simulated time-histories for the two sites are shown in Fig. 3. The assumption of uniform excitation at the bottom of the bridge piers has been made and is deemed reasonable as it would affect the magnitude of the selected engineering demand parameters, but not the overall correlation reduction considerations.

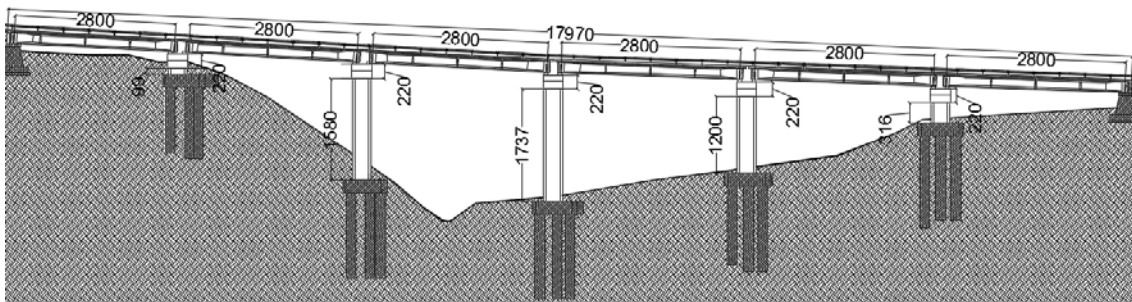


Fig. 2 – Vertical profile of the reinforced concrete bridge located at sites  $\alpha$  and  $\beta$ .

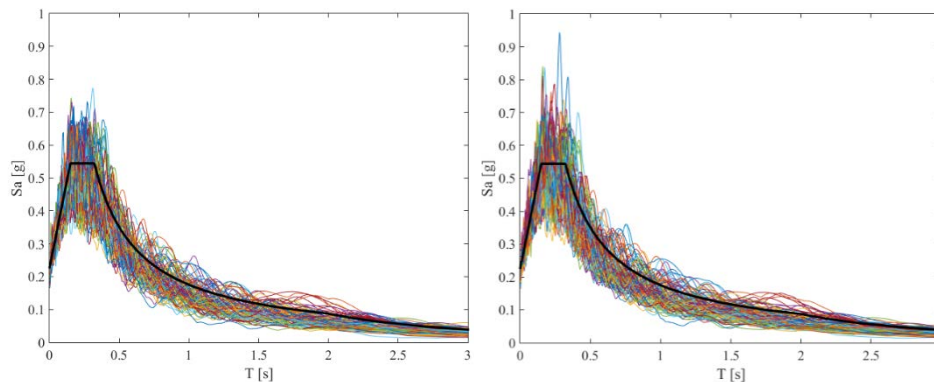


Fig. 3 – Design response (black line) and response spectra at  $\alpha$  site (left hand side) and  $\beta$  site (right hand side).

These two structures were chosen for their general characteristics of regularity. They are multi-span bridges with regular prismatic geometry. Each bridge features 6 spans, each of about 30.5m length, for a total length of 179m. The hollow circular piers vary in height from about 1.0m to 17.4m as depicted in Fig. 2. The deck slope of 5.24% has been considered in the model, whilst the in-plan curvature has been neglected for the sake of simplicity of the configuration.

#### 4.1 Bridge modeling

The bridge has been modelled using the finite element program SeismoStruct [22]. The general configuration is made up of cantilever piers with shear transfer to the deck. The piers are fully fixed to the ground, ignoring soil-structure interaction, whilst the abutments are modelled through four springs in parallel [23], connected through rigid arms, as represented in Fig. 4.

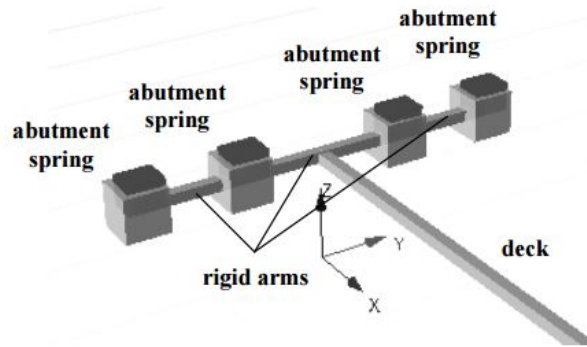


Fig. 4 – Abutment modelling scheme

The deck is composed of three precast prestressed concrete I-beams below a cast-in-place reinforced concrete slab, and was modelled as an elastic element with properties indicated in Table 1. Distributed masses are derived from gravity loads to which lumped masses of 2.28ton/m were added to the deck to include sidewalks, barriers and asphalt. The cap-beams’ and diaphragms’ contribution to the seismic mass was evaluated as 136ton lumped at the pier tops.

Table 1 – Bridge deck properties

Geometrical properties		Material properties	
Parameter	Value	Parameter	Value
A [m <sup>2</sup> ] - Cross section area	3.5868	EA [KN] - Axial stiffness	89·10 <sup>6</sup>
J [m <sup>4</sup> ] - Torsional constant	0.0760	EI <sub>x-x</sub> [KNm <sup>2</sup> ] - Flexure stiffness around x axis	39·10 <sup>6</sup>
I <sub>x-x</sub> [m <sup>4</sup> ] - Inertia moment around x axis	1.5789	EI <sub>y-y</sub> [KNm <sup>2</sup> ] - Flexure stiffness around y axis	639·10 <sup>6</sup>
I <sub>y-y</sub> [m <sup>4</sup> ] - Inertia moment around y axis	25.485	GJ [KNm <sup>2</sup> ] - Torsional stiffness	7.9·10 <sup>6</sup>
-	-	λ [tonnes/m] - mass per unit of length	7.9·10 <sup>6</sup>

The piers present a hollow circular cross section of external and internal diameters of, respectively, 2.8m and 2.2m, reinforced externally and internally with 20ϕ16 rebars at each side. Piers are modelled using force-based elements with 5 integration points and 200 fibers, in order to guarantee sufficient accuracy in the response at global and local levels. Deck-pier connections were modelled with a single node, releasing the appropriate degrees of freedom in order to simulate simple supported conditions. With respect to material modelling, the concrete behavior is represented by the Mander Confined [24] stress-strain model, whilst for the reinforcing steel the model proposed by Menegotto-Pinto [25] was adopted. All the material property details are indicated in Table 2.

#### 4.2 Damage limit states

The definition of the damage limit states is fundamental for the development of fragility curves, as they represent the thresholds to discriminate if a certain structure, under a certain seismic excitation, summarized by a specific IM level, experiences the associated damage level. For the assessment of bridge vulnerability, different damage limit state definitions can be found in literature referring to either single bridge components or global damage impact on the structure. Especially in the case of assessment of a bridge population, a global damage indicator seems to be more convenient and appropriate [9]. The quantitative measures of the damage limit states adopted in the present study are associated with the qualitative limit states defined and used in the



Table 2 – Material properties.

Concrete		Reinforcing Steel	
Parameter	Value	Parameter	Value
$f'_c$ [MPa] - Mean compressive strength	30	$f_y$ [MPa] - Mean yield strength	430
-	-	$f_u$ [MPa] - Mean ultimate strength	485.90
$E_c$ [MPa] – Young Modulus	25'743	$E_s$ [GPa] - Elasticity Modulus	200
$\nu$ - Poisson Ratio	0.2	$\nu$ - Poisson Ration	0.3
$\epsilon_{c0}$ [ $\mu\epsilon$ ] - Strain at peak stress	1960	$\epsilon_y$ [ $\mu\epsilon$ ] - Yield strain	2150
-	-	$\epsilon_u$ [mm/mm] - Fracture strain	0.1
$\gamma_c$ [KN/m <sup>3</sup> ]- Specific weight	24.0	$\gamma_s$ [KN/m <sup>3</sup> ] - Specific weight	78

FEMA loss assessment package HAZUS-MH [26] and have been proposed by Nielson et al, 2005 [27]. The chosen engineering demand parameter (EDP) used for damage quantification was curvature ductility [28], defined as the ratio of maximum column curvature recorded from the nonlinear response analysis to the yield curvature ductility obtained by moment-curvature analysis, as representative of the behavior of the entire bridge. Among the four proposed damage levels (Slight, Moderate, Extensive and Complete), only Slight and Moderate levels have been taken into account, corresponding to 1.29 and 2.10 curvature ductility, respectively. Extensive and collapse damage levels were not included in this study as the selected seismic records were seen not to excite the structures enough to lead to such damage levels. The values of all the curvature ductility ratios were calculated for the case study, under the 100 earthquake excitations, and then compared with the damage limit states. Note, however, that the improvement of the definition of possible damage limit states is beyond the scope of the present paper.

#### 4.3 Nonlinear response analyses and vulnerability characterization

In order to assess the seismic performance of the bridge under the seismic excitation, 100 nonlinear response analyses have been carried out at each location and the curvature ductility has been obtained for each simulated record. The comparison between the two considered damage limit states and the bridge responses allowed assignment of the damage state  $s$  to each bridge site.

### 5. Results and conclusions

This paper presents an investigation into the loss in damage correlation of structures located at different sites when reducing the entire time history to a scalar IM. The inclusion of seismic input correlations has been ensured by the generation of seismic record sets at different locations according to the model described in Section 2. From the 100 simulated time histories for sites  $\alpha$  and  $\beta$ , six IMs, chosen among the optimal IMs for bridge populations [9] were extracted: PGA,  $S_a(T)$ , Fajfar Index [29], root mean square acceleration (aRMS), spectrum intensity (SI) [30], and the index proposed by Vamvatsikos et al. [31],  $N_p$ , which considers spectral accelerations at different periods of vibration. The IM ranges are narrow due to the fact the seismic records have been selected to match a specific PSD, which in turn, corresponds to a target design spectrum. For this reason, the IMs are part of one single IM level. The chosen engineering demand parameter is the curvature ductility and it has been derived for each simulation. IMs and EDP trends are plotted in Fig. 5 and Fig. 6, respectively.

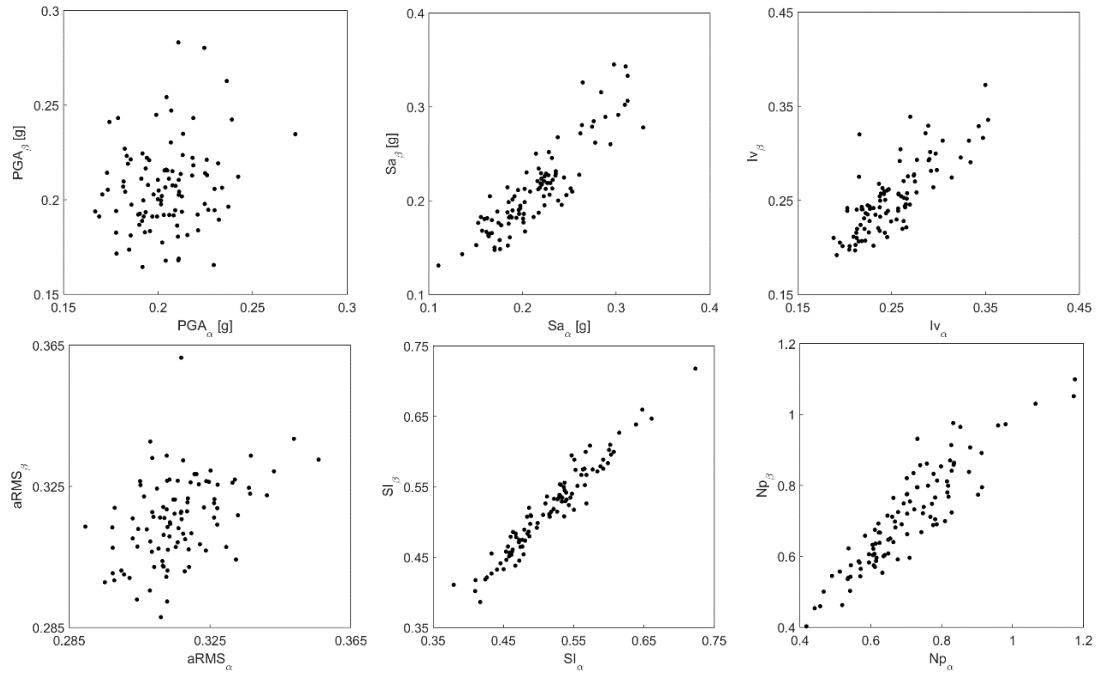


Fig. 5 – IMs corresponding to the 100 earthquake records at  $\alpha$  site (x axis) and  $\beta$  site (y axis)

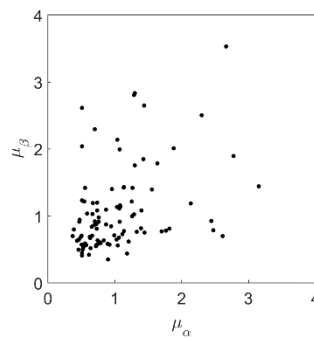


Fig. 6 – Curvature ductility corresponding to the 100 earthquake records at  $\alpha$  site (x axis) and  $\beta$  site (y axis)

The comparison between EDP values and a certain DLS threshold allowed the identification of the damage state for each simulation at each location, leading to the marginal probabilities of exceeding the considered DLSs,  $p_f$ , and correlation factors,  $\rho$ , associated with the two-bridge systems. The evaluated corresponding confidence interval (CI) of the system's damage probabilities were derived either in case of a system in series,  $p_{series}$ , or a system in parallel,  $p_{parallel}$ . The corresponding values represented in Fig. 7 and Fig. 8, and presented in Table 3 of the Appendix, are taken as reference (ref.) values for the purposes of results comparison, being derived through nonlinear dynamic responses. Following the procedure outlined in Section 3, from the obtained resampled dataset, the marginal probabilities of exceeding DLS1 and DLS2,  $p_f$  and corresponding correlation factors,  $\rho$ , were computed. The associated confidence intervals for each IM, DLS and system type are shown in Fig. 7 and Fig. 8, whilst the values are collected in Tables 4 and 5 of the Appendix.

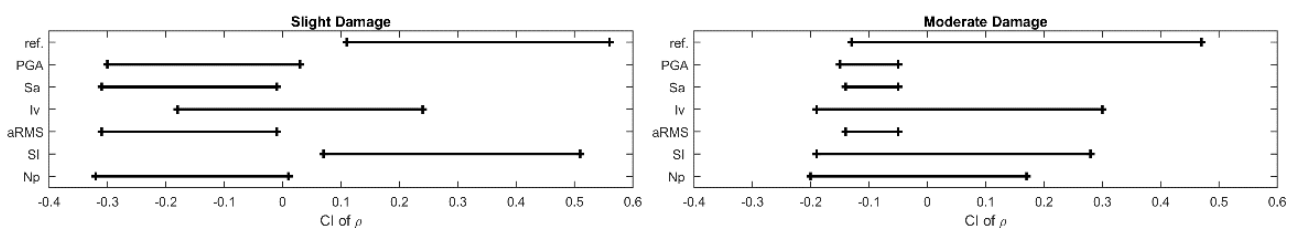


Fig. 7 – Correlation coefficient CIs associated with  $\rho$  for slight (left) and moderate damage (right) and different IMs

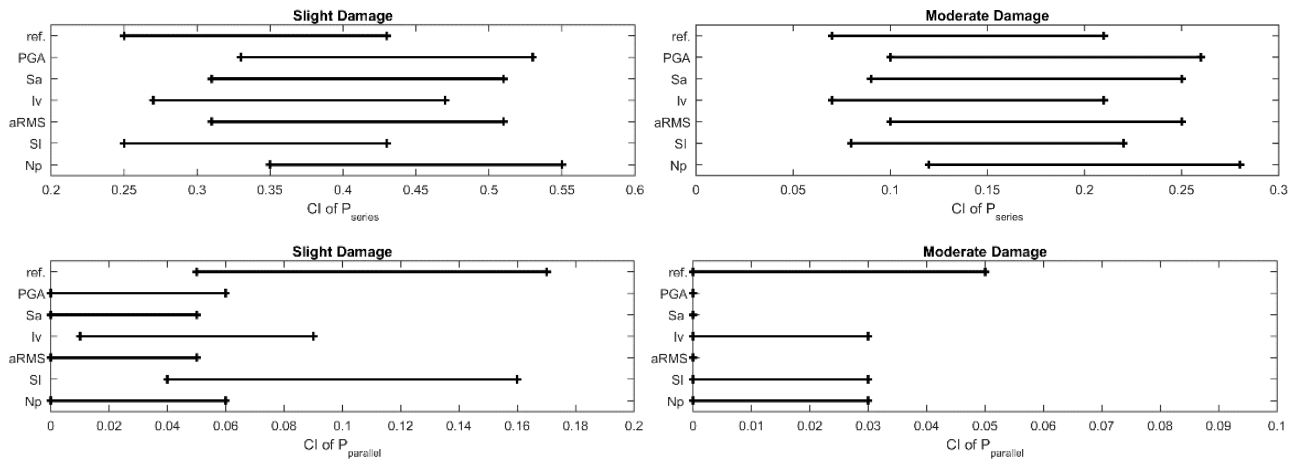


Fig. 8 – Parallel and series systems’ probability of failure for slight (left) and moderate damage (right) and different IMs

The results in Fig. 7 demonstrate how the damage correlation between the two bridges at different locations has decreased when considering different IMs obtained from simulated correlated time histories at those sites, leading in certain cases to negative correlation. Further investigations and a greater number of simulations should be included in future developments of this work in order to better scrutinize negative correlation results. Furthermore, the outcome of this study seems to indicate the heterogeneous probability and correlation trends for the different IMs. In fact, for example, in case of slight damage, SI seems to be able to capture the observed frequencies associated with the nonlinear response analyses, whilst when focusing on moderate damage, SI and Iv provide the closer results. In addition, comparing Fig. 5, 7, and 8, it is interesting to note that the SI metric seems the most correlated in Fig. 5, and it is the most similar to the reference values in Fig. 6 and Fig. 7. On the other hand, the data trends of the other IMs exhibit a general underestimation of the frequencies of all bridges being undamaged and overestimation when one or both bridges are damaged. Moreover, the general trend of parallel and series systems’ data suggests, respectively, underestimation and overestimation of probability of failures due to correlation reduction.

Summarizing, the present work includes the description of a methodology capable of simulating correlated time histories at different sites and the observation that the damage correlation is not being kept even though the seismic input is defined and synthesized in an IM. In order to overcome the limitations due to representing earthquake time histories through a certain IM, future developments could consider the possibility of using PSD functions to link seismic demand and system damage estimates. Alternatively, optimal IMs, identified as those that exhibit less correlation reduction, could be preferred. Future developments of the present work could also include a greater number of simulations, the use of similar, not identical, bridge structures at the different locations and the extension of these investigations to systems with a greater number of components.

## 6. References

- [1] Bensi MT (2010). A Bayesian network methodology for infrastructure seismic risk assessment and decision support. PhD Thesis. Department of Civil and Environmental Engineering, University of California, Berkeley.
- [2] Zelaschi C, Monteiro R, Pinho R (2016): Parametric characterization of RC bridges for seismic assessment purposes. *Structures*, **7**, 14-24.
- [3] Choi E, DesRoches R, Nielson B (2004): Seismic fragility of typical bridges in moderate seismic zones. *Engineering Structures*, **26**, 187-199.
- [4] Nielson BG, DeRoches R (2007): Analytical seismic fragility curves for typical bridges in the central and southeastern United States. *Earthquake Spectra*, **23**, 615-633.
- [5] Pitilakis K, Crowley H, Kaynia A (2014): SYNER-G: Typology definition and fragility functions for physical elements at seismic risk: buildings, lifelines, transportation networks and critical facilities. Springer Science & Business Media.
- [6] Padgett JE, DesRoches R (2008): Methodology for the development of analytical fragility curves for retrofitted bridges. *Earthquake Engineering and Structural Dynamics*, **37**(8), 1157-1174.



- [7] Padgett JE, DesRoches R, M.EERI (2009): Retrofitted Bridge Fragility Analysis for Typical Classes of Multispan Bridges. *Earthquake Spectra*, **25**<sup>o</sup>(1), 117-141.
- [8] Soleimani FS, DesRoches RD, Padgett JE (2016): Development of fragility curves for bridges with irregular configurations. IFIP WG-7.5 Reliability and Optimization of Structural Systems, Pittsburgh, PA.
- [9] Zelaschi C, Monteiro R, Pinho R (2015): Improved fragility functions for RC bridge populations. 5th ECCOMAS Thematic Conference on Computational Methods in Structural Dynamics and Earthquake Engineering (COMPDYN 2015), Crete Island, Greece.
- [10] Zelaschi C, Monteiro R, Marques M, Pinho R (2014): Comparative analysis of intensity measures for reinforced concrete bridges. 2nd European conference on Earthquake Engineering and Seismology, Istanbul, Turkey.
- [11] Goda K, Hong HP (2008): Spatial correlation of peak ground motions and response spectra. *Bulletin of Seismological Society of America*, **98**<sup>o</sup>(1), 354-365.
- [12] Boore DM, Gibbs JF, Joyner WB, Tinsley JC, Ponti DJ (2003): Estimated ground motion from the 1994 Northridge, California, earthquake at the site of the Interstate 10 and La Cienega Boulevard bridge collapse, West Los Angeles, California. *Bulletin of the Seismological Society of America*, **93**<sup>o</sup>(6), 2737-2751.
- [13] Wang M, Takada T (2005): Macrospatial correlation model of seismic ground motions. *Earthquake Spectra*, **21**<sup>o</sup>(4), 1137-1156.
- [14] Baker JW, Jayaram N (2008): Correlation of spectral acceleration values from NGA ground motion models. *Earthquake Spectra*, **24**<sup>o</sup>(1), 299-317.
- [15] Jayaram N, Baker JW (2009): Correlation model for spatially distributed ground-motion intensities. *Earthquake Engineering and Structural Dynamics*, **38**<sup>o</sup>(15), 1687-1708.
- [16] Loth C, Baker JW (2010): A spatial cross-correlation model of spectral accelerations at multiple periods. *Earthquake Engineering and Structural Dynamics*, **42**<sup>o</sup>(3), 397-417.
- [17] Foulser-Piggot R, Stafford PJ (2012): A predictive model for Arias intensity at multiple sites and consideration of spatial correlations. *Earthquake Engineering and Structural Dynamics*, **41**<sup>o</sup>, 431-451.
- [18] Esposito S, Iervolino I (2011): PGA and PGV spatial correlation models based on European multievent datasets. *Bulletin of the Seismological Society of America*, **101**<sup>o</sup>(5), 2532-2541.
- [19] Der Kiureghian A (1996): A coherency model for spatially varying ground motions. *Earthquake Engineering and Structural Dynamics*, **25**<sup>o</sup>, 99-111.
- [20] Konakli K, Der Kiureghian A (2012): Simulation of spatially varying ground motions including incoherence, wave-passage and differential site-response effects. *Earthquake Engineering and Structural Dynamics*, **41**<sup>o</sup>, 495-513.
- [21] Malings C, Pozzi M (2016): Conditional Entropy and Value of Information Metrics for Optimal Sensing in Infrastructure Systems. *Structural Safety*, **60**<sup>o</sup>: 77-90.
- [22] SeismoStruct v7.0 (2014); A computer program for static and dynamic nonlinear analysis of framed structures. Available from <http://www.seismosoft.com>.
- [23] Monteiro R (2016): Sampling based numerical seismic assessment of continuous span RC bridges. *Engineering Structures*, **118**<sup>o</sup>, 407-420.
- [24] Mander JB, Priestley MJN and Park R (1998): Theoretical stress-strain model for confined concrete. *Journal of Structural Engineering*, **114**<sup>o</sup>(8), 1804-1826.
- [25] Menegotto M, Pinto PE (1973): Method of analysis for cyclically loaded R.C. plane frames including changes in geometry and non-elastic behaviour of elements under combined normal force and bending. Symposium on the Resistance and Ultimate Deformability of Structures Acted on by Well Defined Repeated Loads, International Association for Bridge and Structural Engineering, Zurich, Switzerland, 15-22.
- [26] FEMA (Federal Emergency Management Agency, Department of Homeland Security Emergency Preparedness and Response Directorate) (2003): HAZUS-MH MR3, Technical Manual.
- [27] Nielson BG (2005): Analytical fragility curves for highway bridges in moderate seismic zones. PhD thesis. School of Civil and Environmental Engineering, Georgia Institute of Technology, Atlanta, USA.
- [28] Plevris V, Mitropoulou CC, Lagaros ND (2012): Structural seismic design optimization and earthquake engineering: formulations and applications, IGI Global.
- [29] Fajfar P, Vidic T and Fishinger M (1990): A measure of earthquake motion capacity to damage medium-period structures. *Soil Dynamics and Earthquake Engineering*, **9**<sup>o</sup>(5):236-242.



[30] Kramer SL (1995): Geotechnical Earthquake Engineering. Prentice Hall, Inc.

[31] Vamvatsikos D, Cornell CA (2005): Developing efficient scalar and vector intensity measures for IDA capacity estimation by incorporating elastic spectral shape information. Earthquake Engineering and Structural Dynamics, 34(13), 1573-1600.

## 6. Appendix

Table 3 – Damage probabilities from 100 simulations for slight (DLS1) and moderate (DLS2) damage.

-	Observed frequencies			95% CI of $p_f$	95% CI of $\rho$	95% CI of $P_{series}$	95% CI of $P_{parallel}$
	0	1	2				
# of damaged bridges							
<b>Slight</b>	0.66	0.23	0.11	[0.16; 0.29]	[0.11; 0.56]	[0.25; 0.43]	[0.05; 0.17]
<b>Moderate</b>	0.86	0.12	0.02	[0.04; 0.12]	[-0.13; 0.47]	[0.07; 0.21]	[0; 0.05]

Table 4 – Sampled damage probabilities for slight (DLS1) damage

-	Observed frequencies			95% CI of $p_f$	95% CI of $\rho$	95% CI of $P_{series}$	95% CI of $P_{parallel}$
	0	1	2				
# of damaged bridges							
<b>PGA</b>	0.57	0.40	0.03	[0.18; 0.29]	[-0.30; 0.03]	[0.33; 0.53]	[0; 0.06]
<b>Sa</b>	0.59	0.39	0.02	[0.16; 0.27]	[-0.31; -0.01]	[0.31; 0.51]	[0; 0.05]
<b>Iv</b>	0.63	0.32	0.05	[0.15; 0.27]	[-0.18; 0.24]	[0.27; 0.47]	[0.01; 0.09]
<b>aRMS</b>	0.59	0.39	0.02	[0.16; 0.27]	[-0.31; -0.01]	[0.31; 0.51]	[0; 0.05]
<b>SI</b>	0.66	0.24	0.10	[0.15; 0.29]	[0.07; 0.51]	[0.25; 0.43]	[0.04; 0.16]
<b>Np</b>	0.55	0.42	0.03	[0.18; 0.30]	[-0.32; 0.01]	[0.35; 0.55]	[0; 0.06]

Table 5 – Sampled damage probabilities for moderate (DLS2) damage

-	Observed frequencies			95% CI of $p_f$	95% CI of $\rho$	95% CI of $P_{series}$	95% CI of $P_{parallel}$
	0	1	2				
# of damaged bridges							
<b>PGA</b>	0.82	0.18	-	[0.05; 0.13]	[-0.15; -0.05]	[0.10; 0.26]	-
<b>Sa</b>	0.83	0.17	-	[0.05; 0.12]	[-0.14; -0.05]	[0.09; 0.25]	-
<b>Iv</b>	0.86	0.13	0.01	[0.04; 0.11]	[-0.19; 0.30]	[0.07; 0.21]	[0; 0.03]
<b>aRMS</b>	0.83	0.17	-	[0.05; 0.12]	[-0.14; -0.05]	[0.10; 0.25]	-
<b>SI</b>	0.85	0.14	0.01	[0.04; 0.12]	[-0.19; 0.28]	[0.08; 0.22]	[0; 0.03]
<b>Np</b>	0.80	0.19	0.01	[0.06; 0.15]	[-0.20; 0.17]	[0.12; 0.28]	[0; 0.03]